PROCEEDINGS OF THE ROYAL SOCIETY A

Proc. R. Soc. A (2009) **465**, 2761–2783
doi:10.1098/rspa.2008.0536
Published online 24 June 2009

On the groundstate energy of tight knots

By Francesca Maggioni[1] and Renzo L. Ricca[2,*]

[1]*Department of Mathematics, Statistics, Computer Science and Applications, U. Bergamo, Via dei Caniana 2, 24127 Bergamo, Italy*
[2]*Department of Mathematics and Applications, U. Milano-Bicocca, Via Cozzi 53, 20125 Milano, Italy*

New results on the groundstate energy of tight, magnetic knots are presented. Magnetic knots are defined as tubular embeddings of the magnetic field in an ideal, perfectly conducting, incompressible fluid. An orthogonal, curvilinear coordinate system is introduced and the magnetic energy is determined by the poloidal and toroidal components of the magnetic field. Standard minimization of the magnetic energy is carried out under the usual assumptions of volume- and flux-preserving flow, with the additional constraints that the tube cross section remains circular and that the knot length (ropelength) is independent from internal field twist (framing). Under these constraints the minimum energy is determined analytically by a new, exact expression, function of ropelength and framing. Groundstate energy levels of tight knots are determined from ropelength data obtained by the SONO tightening algorithm. Results for torus knots are compared with previous work, and the groundstate energy spectrum of the first prime knots — up to 10 crossings — is presented and analysed in detail. These results demonstrate that ropelength and framing determine the spectrum of magnetic knots in tight configuration.

Keywords: magnetic knots; ropelength; magnetic relaxation; ideal shapes; energy minimizer

1. Introduction

Work to establish rigorous relationships between energy and topological complexity of physical systems is of fundamental importance in both pure and applied mathematics. Progress in this direction has been slow, but steady, since Arnold's (1974) original contribution. For magnetic knots, in particular, the problem can be synthesized as follows: if the initial field is confined to a single knotted flux tube of signature $\{V, \Phi\}$ (V magnetic volume and Φ magnetic flux), then the minimal magnetic energy $M_{\min}$ under a signature-preserving flow is given by (Moffatt 1990)

$$M_{\min} = m(h)\Phi^2 V^{-1/3}, \tag{1.1}$$

where $m(h)$ is a positive dimensionless function of the dimensionless twist parameter h. Of particular interest is the value of h for which $m(h)$ is minimal ($m_{\min}$). A fundamental problem here is this (Moffatt 2001):

*Author for correspondence (renzo.ricca@unimib.it).

Received 27 December 2008
Accepted 27 May 2009

Problem 1.1. *Determine* $m_{\min}$ *for knots of minimum crossing number* $3, 4, 5, \ldots$.

Minimization of magnetic energy of knot types bears some analogies with another type of problem that originates from work on the shape of ideal knots (see, for instance, the collection of papers edited by Stasiak *et al.* (1998)). In this context knots are thought of as made by a perfectly flexible and infinitely hard, cylindrical rope closed upon itself; a fundamental question here is given by the following (Litherland *et al.* 1999):

Problem 1.2. *Can you tie a knot in a one-foot length of one-inch rope?*

This problem admits an obvious generalization to knot types of increasing complexity, so that the question can be generalized to finding the minimal length of a given knot type. As we shall see, the two problems tend to coincide at some fundamental level. If the relaxation of magnetic field to minimum energy state occurs under a volume- and flux-preserving flow, then the process, driven by the action of the Lorentz force, resembles the minimal shortening of an infinitely flexible, elastic rope under shrinking deformation. In the incompressible limit, a shrinking, volume-preserving flow acts on the tubular knot by increasing the average tube cross section as the knot length diminishes. Thickening of the fattening knot stops when the topological barrier given by the knot type prevents further relaxation (see §5). For magnetic knots this end-state will have minimal energy *and*, for tight knotted ropes, minimal ropelength. Existence of a positive lower bound for magnetic energy (Freedman 1988), however, is not sufficient to guarantee that a global minimum is actually attained, even in ideal conditions. With increasing knot complexity, for example, configurational arrangements may indeed prevent full relaxation, with local minima of magnetic energy (or ropelength) trapped from further minimization.

In the present paper we shall consider magnetic relaxation subject to the invariance of magnetic signature (volume and flux) with the *a priori* assumption that the magnetic tubular boundary of the flux tube remains circular at all times and that the knot length is independent from the internal twist h. There is certainly no physical reason to expect this to happen, other than mathematical advantage in the analysis of the energy functional. These assumptions pose additional mathematical constraints on the relaxation process, preventing full minimization. However, the information on energy thus found provides, we believe, a reasonable approximation (from above) to the true bound. By this approach we shall demonstrate (theorem 5.2) that magnetic energy minima can be related to the minimal ropelength by an exact, analytical expression (given by equation (5.4), or the simplified form (6.3)) for the minimized constrained magnetic energy of knots. Then, by using minimal length data obtained by the Shrink-On-No-Overlaps (SONO) algorithm (briefly reviewed in §6*a*) ideated by Pieranski (1998) and implemented by Przybyl (2001) and collaborators, we determine the constrained groundstate energy levels of the first 250 prime knots up to 10 crossings (§8). In doing so, we also compare results extrapolated from the SONO data by using equation (6.3) with previous work done by Chui & Moffatt (1995; hereafter denoted by CM95), highlighting the limitations of their approach and commenting on some marked differences in the results. Some critical issues and open problems for future work are discussed in §9.

Figure 1. Magnetic knot given by the tubular embedding of the magnetic field centred on the knot $K_{7.7}$. In ideal conditions knot volume V and magnetic flux Φ are conserved quantities.

2. Magnetic knots as tubular embeddings in ideal fluid

We consider tubular knots as tubular embeddings of the magnetic field in an ideal, incompressible, perfectly conducting fluid in S^3 (i.e. $\mathbb{R}^3 \cup \{\infty\}$, simply connected). The magnetic field $\mathbf{B} = \mathbf{B}(\mathbf{x}, t)$ ($\mathbf{x}$ the position vector and t time) is frozen in the fluid and has finite energy, that is,

$$\mathbf{B} \in \{\nabla \cdot \mathbf{B} = 0, \partial_t \mathbf{B} = \nabla \times (\mathbf{u} \times \mathbf{B}), L_2\text{-norm}\}. \tag{2.1}$$

A magnetic knot K is given by the embedding of the magnetic field in a *regular* tubular neighbourhood $\mathcal{T}_a$ of radius $a > 0$, centred on the knot axis $\mathcal{C}$ of local radius of curvature $\rho > 0$ (see figure 1). The field is actually embedded onto nested tori $\mathcal{T}_i (i = 1, \ldots, n)$ in $\mathcal{T}_a$, and regularity is ensured by taking $a \leq \rho$ pointwise along $\mathcal{C}$. The existence of non-self-intersecting nested tori in $\mathcal{T}_a$ is guaranteed by the tubular neighbourhood theorem (Spivak 1979). $\mathcal{C}$ is assumed to be a C^2-smooth, closed loop (submanifold of S^3 homeomorphic to S^1), simple (i.e. non-self-intersecting) and parametrized by arc-length. The total length of $\mathcal{C}$ is $L = L(\mathcal{C})$. Evidently K has the knot type of $\mathcal{C}$, being either *trivial*, whether $\mathcal{C}$ (an unknot) bounds a smoothly embedded disc, or *essential*. For simplicity we take $\mathcal{T}_a = \mathcal{C} \otimes \mathcal{S}$ given by the product of $\mathcal{C}$ with the solid circular disc $\mathcal{S}$ of area $A = \pi a^2$, taken in the cross-sectional plane to $\mathcal{C}$. The total volume is $V = V(\mathcal{T}_a) = \pi a^2 L$. We assume that the tubular boundary $\partial \mathcal{T}_a = \partial \mathcal{T}$ (dropping the suffix) remains a magnetic circular, cylindrical surface at all times, of uniform cross section all along $\mathcal{C}$; denoting by $\hat{\boldsymbol{\nu}}_\perp$ the unit normal to $\partial \mathcal{T}$, we have $\mathrm{supp}(\mathbf{B}) := K$, where

$$\mathcal{T}(K) \hookrightarrow S^3 \quad \text{with} \quad \mathbf{B} \cdot \hat{\boldsymbol{\nu}}_\perp = 0 \quad \text{on} \quad \partial \mathcal{T}. \tag{2.2}$$

The magnetic flux Φ through the cross section $\mathcal{S}$ is given by

$$\Phi = \int_{A(\mathcal{S})} \mathbf{B} \cdot \hat{\boldsymbol{\nu}} \, \mathrm{d}^2\mathbf{x}, \tag{2.3}$$

where now $\hat{\boldsymbol{\nu}}$ is the unit normal to $\mathcal{S}$. In ideal conditions the knot K evolves under the action of the group of volume- and flux-preserving diffeomorphisms

$\varphi : K \to K_\varphi$. Magnetic energy $M(t)$ and magnetic helicity $H(t)$ are two fundamental physical quantities, defined by

$$M(t) = \frac{1}{2}\int_{V(K)} \|\mathbf{B}\|^2 \, \mathrm{d}^3\mathbf{x}, \tag{2.4}$$

and

$$H(t) = \int_{V(K)} \mathbf{A}\cdot\mathbf{B} \, \mathrm{d}^3\mathbf{x}, \tag{2.5}$$

where $\mathbf{A}$ is the vector (Coulomb) potential associated with $\mathbf{B} = \nabla \times \mathbf{A}$. As usual, we take $\nabla \cdot \mathbf{A} = 0$ in S^3. For frozen fields helicity is a conserved quantity (Woltjer 1958), thus $H(t) = H = \text{constant}$. Moreover, it is well known that helicity admits topological interpretation in terms of linking numbers, and for a single magnetic knot we have (Berger & Field 1984; Moffatt & Ricca 1992):

Theorem 2.1. *Let K be an essential magnetic knot in an ideal fluid. Then*

$$H = Lk\Phi^2 = (\mathrm{Wr} + \mathrm{Tw})\Phi^2, \tag{2.6}$$

where Lk denotes the Călugăreanu–White linking number of $\mathcal{C}$ with respect to the framing induced by the embedding of the $\mathbf{B}$-lines in $\mathcal{T}$.

The two *geometric* quantities Wr and Tw are the writhing number and the twist number: Wr is a measure of the average coiling and distortion of $\mathcal{C}$ in space and depends only on the geometry of $\mathcal{C}$, while Tw measures the winding of the field-lines around $\mathcal{C}$, thus depending on the embedding of the $\mathbf{B}$-lines within $\mathcal{T}$. *Zero-framing* of the field lines denotes zero-linking ($Lk = 0$) of these lines with $\mathcal{C}$, thus providing a reference measure for helicity calculations (see appendix A).

3. Curvilinear coordinate system

It is useful to adopt an orthogonal curvilinear system of coordinates centred on $\mathcal{C}$. Let $\mathcal{C}$ be parametrized by the equation $\mathbf{x} = \mathbf{X}(s)$, where s is arc-length, with origin $s = 0$ at some point $O \in \mathcal{C}$. Let $\hat{\mathbf{t}}(s) = \mathbf{X}'(s)$ be the unit tangent to $\mathcal{C}$, prime denoting arc-length derivative. We take $\mathcal{C}$ to be inflexion-free, then $\hat{\mathbf{n}}(s)$ and $\hat{\mathbf{b}}(s)$ are, respectively, the standard unit normal and binormal to $\mathcal{C}$, with curvature $c = c(s) = 1/\rho(s)$ and torsion $\tau = \tau(s)$ given by the standard Frenet–Serret equations, i.e.

$$\hat{\mathbf{t}}' = c\hat{\mathbf{n}}, \quad \hat{\mathbf{n}}' = -c\hat{\mathbf{t}} + \tau\hat{\mathbf{b}}, \quad \hat{\mathbf{b}}' = -\tau\hat{\mathbf{n}}. \tag{3.1}$$

If $c(s) = 0$ at some point of $\mathcal{C}$, then $\mathcal{C}$ has there an inflexion and $\hat{\mathbf{n}}(s)$ is undefined. Because $\mathcal{C}$ is assumed to be C^2-smooth, local inflexional configurations will be resolved by a continuity argument from either side of the inflexion point. Thus, without loss of generality, we shall take $\mathcal{C}$ to be inflexion-free, that is

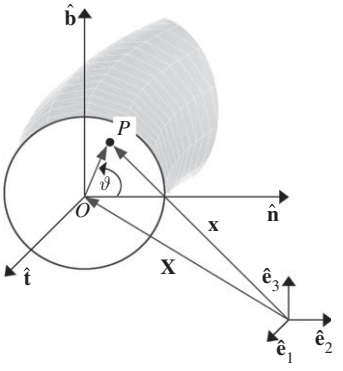

Figure 2. Relationship between fixed reference frame and the Frenet frame $\{\hat{\mathbf{t}}, \hat{\mathbf{n}}, \hat{\mathbf{b}}\}$ for a point P in the tube cross section $\mathcal{S}$.

$c(s) > 0$, $\forall s \in [0, L]$, so that the Frenet triad $\{\hat{\mathbf{t}}, \hat{\mathbf{n}}, \hat{\mathbf{b}}\}$ is everywhere well defined on $\mathcal{C}$. A point $P \in \mathcal{S}$ (see figure 2) is thus given by

$$\mathbf{x} = \mathbf{X}(s) + r\cos\vartheta\,\hat{\mathbf{n}}(s) + r\sin\vartheta\,\hat{\mathbf{b}}(s), \tag{3.2}$$

where (r, ϑ) is the polar coordinate system in the cross-sectional plane.

Lemma 3.1. *Let $\mathcal{T}$ be a regular tubular neighbourhood of $\mathcal{C}$. Then the system of coordinates $(r, \vartheta_{\mathrm{R}}, s)$, where*

$$\vartheta_{\mathrm{R}} = \vartheta + \int_0^s \tau(\bar{s})\,\mathrm{d}\bar{s}, \tag{3.3}$$

provides a zero-twist reference system on $\mathcal{C}$ in $\mathcal{T}$.

Proof. Let us consider a second curve $\mathcal{C}^*$, of equation

$$\mathbf{X}^*(s) = \mathbf{X}(s) + r\hat{\mathbf{T}}_2(s), \tag{3.4}$$

parallel transfer of $\mathcal{C}$ at a distance r in the normal direction along $\hat{\mathbf{T}}_2 = \hat{\mathbf{n}}\cos\vartheta^* + \hat{\mathbf{b}}\sin\vartheta^*$; $\mathcal{C}^*$ is a 'push-off' of $\mathcal{C}$ in the normal direction $\hat{\mathbf{T}}_2$. The pair $\{\mathcal{C}, \mathcal{C}^*\}$ identifies the ribbon $\mathcal{R}(\mathcal{C}, \mathcal{C}^*)$ of edges $\mathbf{X}(s)$ and $\mathbf{X}^*(s)$, whose twist provides a measure of the winding of $\mathcal{C}^*$ around $\mathcal{C}$. For a generic infinitesimal displacement of the point $P \in \mathcal{S}$ (see figure 2) in space, we have

$$\mathrm{d}\mathbf{x} = \left(\hat{\mathbf{t}} + \xi_2\frac{\mathrm{d}\hat{\mathbf{T}}_2}{\mathrm{d}s} + \xi_3\frac{\mathrm{d}\hat{\mathbf{T}}_3}{\mathrm{d}s}\right)\mathrm{d}s + \hat{\mathbf{T}}_2\,\mathrm{d}\xi_2 + \hat{\mathbf{T}}_3\,\mathrm{d}\xi_3, \tag{3.5}$$

where ξ_2, ξ_3 denote coordinates along $\hat{\mathbf{T}}_2$ and $\hat{\mathbf{T}}_3 = -\hat{\mathbf{n}}\sin\vartheta^* + \hat{\mathbf{b}}\cos\vartheta^*$, respectively. Note that the triple $\{\hat{\mathbf{t}}, \hat{\mathbf{T}}_2, \hat{\mathbf{T}}_3\}$ is orthogonal. By using equation (3.1), we have

$$\begin{aligned}\mathrm{d}\mathbf{x} = &\left[(1 - \xi_2 c\cos\vartheta^* + \xi_3 c\sin\vartheta^*)\hat{\mathbf{t}} + \left(\tau + \frac{\mathrm{d}\vartheta^*}{\mathrm{d}s}\right)\left(\xi_2\hat{\mathbf{T}}_3 - \xi_3\hat{\mathbf{T}}_2\right)\right]\mathrm{d}s \\ &+ \hat{\mathbf{T}}_2\,\mathrm{d}\xi_2 + \hat{\mathbf{T}}_3\,\mathrm{d}\xi_3.\end{aligned} \tag{3.6}$$

Hence, the metric is given by

$$\mathrm{d}\mathbf{x}\cdot\mathrm{d}\mathbf{x}=\left[\left(1-\xi_2 c\cos\vartheta^*+\xi_3 c\sin\vartheta^*\right)^2+(\xi_2^2+\xi_3^2)\left(\tau+\frac{\mathrm{d}\vartheta^*}{\mathrm{d}s}\right)\right](\mathrm{d}s)^2$$
$$+(\mathrm{d}\xi_2)^2+(\mathrm{d}\xi_3)^2+2\left(\tau+\frac{\mathrm{d}\vartheta^*}{\mathrm{d}s}\right)(\xi_2\,\mathrm{d}\xi_3-\xi_3\,\mathrm{d}\xi_2). \tag{3.7}$$

The metric is orthogonal in the following cases:

$$\text{(i)}\quad \tau+\frac{\mathrm{d}\vartheta^*}{\mathrm{d}s}=0\quad\text{or}\quad\text{(ii)}\quad \xi_2\,\mathrm{d}\xi_3-\xi_3\,\mathrm{d}\xi_2=0. \tag{3.8}$$

Condition (ii) corresponds to a degenerate system of coordinates, since $\xi_2=\xi_3+\text{const.}$; condition (i) provides zero twist of the reference system $\{\hat{\mathbf{t}},\hat{\mathbf{T}}_2,\hat{\mathbf{T}}_3\}$ everywhere along $\mathcal{C}$, since (cf. Moffatt & Ricca 1992)

$$Tw=\frac{1}{2\pi}\int_{\mathcal{C}}\left(\tau(s)+\frac{\mathrm{d}\vartheta^*(s)}{\mathrm{d}s}\right)\mathrm{d}s. \tag{3.9}$$

Integration of equation (3.8)(i) gives

$$\vartheta^*(s)=-\int_0^s\tau(\bar{s})\,\mathrm{d}\bar{s}+\vartheta_0; \tag{3.10}$$

without loss of generality we take $\vartheta_0=0$, so that $\mathcal{R}(\mathcal{C},\mathcal{C}^*)$ spans pointwise in the normal direction given by the push-off of $\mathcal{C}^*$; the pair $\{\mathcal{C},\mathcal{C}^*\}$ is untwisted and provides *zero-twist* for the coordinate system. Hence, the metric is orthogonal and it is given by

$$\mathrm{d}\mathbf{x}\cdot\mathrm{d}\mathbf{x}=[1-c(\xi_2\cos\vartheta^*-\xi_3\sin\vartheta^*)]^2(\mathrm{d}s)^2+(\mathrm{d}\xi_2)^2+(\mathrm{d}\xi_3)^2, \tag{3.11}$$

and by taking

$$\xi_2=r\cos\vartheta_{\mathrm{R}}\quad\text{and}\quad\xi_3=r\sin\vartheta_{\mathrm{R}}, \tag{3.12}$$

we have

$$\mathrm{d}\mathbf{x}\cdot\mathrm{d}\mathbf{x}=[1-cr\cos(\vartheta_{\mathrm{R}}+\vartheta^*)]^2(\mathrm{d}s)^2+(\mathrm{d}r)^2+r^2(\mathrm{d}\vartheta_{\mathrm{R}})^2. \tag{3.13}$$

By using equation (3.10), the independent coordinate ϑ_{R} is related to the polar angle ϑ by

$$\vartheta_{\mathrm{R}}=\vartheta+\int_0^s\tau(\bar{s})\,\mathrm{d}\bar{s}. \tag{3.14}$$

■

The orthogonal system $(r,\vartheta_{\mathrm{R}},s)$ was originally found by Mercier (1963). In the orthonormal basis $\{\hat{\mathbf{e}}_r,\hat{\mathbf{e}}_{\vartheta_{\mathrm{R}}},\hat{\mathbf{t}}\}$ the scale factors h_1,h_2,h_3 are given by

$$\left.\begin{aligned}\frac{\partial\mathbf{x}}{\partial r}&=h_1\hat{\mathbf{e}}_r=\cos\vartheta(\vartheta_{\mathrm{R}},s)\hat{\mathbf{n}}(s)+\sin\vartheta(\vartheta_{\mathrm{R}},s)\hat{\mathbf{b}}(s),\\ \frac{\partial\mathbf{x}}{\partial\vartheta_{\mathrm{R}}}&=h_2\hat{\mathbf{e}}_{\vartheta_{\mathrm{R}}}=-r\sin\vartheta(\vartheta_{\mathrm{R}},s)\hat{\mathbf{n}}(s)+r\cos\vartheta(\vartheta_{\mathrm{R}},s)\hat{\mathbf{b}}(s),\\ \frac{\partial\mathbf{x}}{\partial s}&=h_3\hat{\mathbf{t}}=(1-c(s)r\cos\vartheta(\vartheta_{\mathrm{R}},s))\hat{\mathbf{t}}(s).\end{aligned}\right\} \tag{3.15}$$

By setting $k = k(r, \vartheta_{\mathrm{R}}, s) = 1 - c(s) r \cos\vartheta(\vartheta_{\mathrm{R}}, s)$, the metric tensor is given by

$$(g_{i,j}) = (h_i \hat{\mathbf{e}}_i) \cdot (h_j \hat{\mathbf{e}}_j) = \begin{pmatrix} 1 & 0 & 0 \\ 0 & r^2 & 0 \\ 0 & 0 & k^2 \end{pmatrix},$$

where $\hat{\mathbf{e}}_1 = \hat{\mathbf{e}}_r, \hat{\mathbf{e}}_2 = \hat{\mathbf{e}}_{\vartheta_{\mathrm{R}}}, \hat{\mathbf{e}}_3 = \hat{\mathbf{t}}$, with determinant $g = r^2 k^2$, and Jacobian

$$J = (h_1 \hat{\mathbf{e}}_r \cdot h_2 \hat{\mathbf{e}}_{\vartheta_{\mathrm{R}}}) \times h_3 \hat{\mathbf{t}} = \sqrt{g} = rk. \tag{3.16}$$

Because we assume that $r < c^{-1} = \rho$, we have $J > 0$ so that the transformation is well defined. Hence, equation (3.2) reduces to

$$\mathbf{x} = \mathbf{X}(s) + r\hat{\mathbf{e}}_r \quad \text{with} \quad \vartheta = \vartheta_{\mathrm{R}} - \int_0^s \tau(\bar{s})\, \mathrm{d}\bar{s}. \tag{3.17}$$

4. Magnetic field and flux prescription

As $\partial\mathcal{T}$ is a magnetic surface, the magnetic field $\mathbf{B}$ is given purely in terms of poloidal and toroidal components, that is,

$$\mathbf{B} = \mathbf{B}_{\mathrm{P}} + \mathbf{B}_{\mathrm{T}} = B_{\vartheta_{\mathrm{R}}} \hat{\mathbf{e}}_{\vartheta_{\mathrm{R}}} + B_s \hat{\mathbf{t}}. \tag{4.1}$$

Moreover, as $\mathbf{B}$ is divergenceless, we have

$$\nabla \cdot \mathbf{B} = \frac{1}{rk}\left[\frac{\partial(kB_{\vartheta_{\mathrm{R}}})}{\partial\vartheta_{\mathrm{R}}} + \frac{\partial(rB_s)}{\partial s}\right] = 0, \tag{4.2}$$

so that there exists a flux function $\psi(r, \vartheta_{\mathrm{R}}, s)$, such that

$$B_{\vartheta_{\mathrm{R}}} = \frac{1}{k}\frac{\partial\psi}{\partial s}, \quad B_s = -\frac{1}{r}\frac{\partial\psi}{\partial\vartheta_{\mathrm{R}}}. \tag{4.3}$$

For the magnetic field to be single-valued, $\psi(r, \vartheta_{\mathrm{R}}, s)$ must be the sum of terms that are either linear or periodic in ϑ_{R} and s (cf. Bateman 1978, pp. 127–128); hence, periodicity in both coordinates may be prescribed.

We now need to express the magnetic field in terms of toroidal and poloidal flux. Let Φ_{T} be the toroidal flux through a cross-sectional area of $\mathcal{T}$ of radius r (see figure 3*a*),

$$\Phi_{\mathrm{T}} = \int_0^r \int_0^{2\pi} B_s \bar{r}\, \mathrm{d}\vartheta_{\mathrm{R}} \mathrm{d}\bar{r}. \tag{4.4}$$

From the second equation (4.3) and the periodicity of ψ in ϑ_{R}, we have

$$\Phi_{\mathrm{T}}(r) = -2\pi \int_0^r \frac{\partial\psi}{\partial\vartheta_{\mathrm{R}}}\, \mathrm{d}\bar{r}; \tag{4.5}$$

hence

$$\psi(r, \vartheta_{\mathrm{R}}, s) = -\frac{\vartheta_{\mathrm{R}}}{2\pi}\frac{\mathrm{d}\Phi_{\mathrm{T}}(r)}{\mathrm{d}r} + c_1(r, s). \tag{4.6}$$

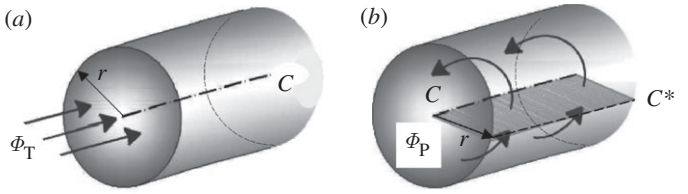

Figure 3. (*a*) Toroidal and (*b*) poloidal flux in $\mathcal{T}$.

The poloidal flux Φ_P through a ribbon area of width r (see figure 3*b*) is given by

$$\Phi_P = \int_0^{L/k} \int_0^r B_{\vartheta_R} \, d\bar{r} k \, ds. \tag{4.7}$$

From the first equation (4.3) and the periodicity of ψ in s, we have

$$\Phi_P(r) = \int_0^r \frac{L}{k} \frac{\partial \psi}{\partial s} \, d\bar{r}, \tag{4.8}$$

so that

$$\psi(r, \vartheta_R, s) = \frac{s}{L} \frac{d\Phi_P(r)}{dr} + c_2(r, \vartheta_R). \tag{4.9}$$

Thus, from equations (4.6) and (4.9), we have

$$\psi(r, \vartheta_R, s) = -\frac{\vartheta_R}{2\pi} \frac{d\Phi_T(r)}{dr} + \frac{s}{L} \frac{d\Phi_P(r)}{dr} + \tilde{\psi}(r, \vartheta_R, s), \tag{4.10}$$

where $\tilde{\psi} = \tilde{\psi}(r, \vartheta_R, s) = c_1(r, s) + c_2(r, \vartheta_R)$ is a single-valued function, periodic in ϑ_R (with period 2π) and in s (with period L). By equations (4.3), we have

$$\mathbf{B} = \left(0, \frac{1}{L} \frac{d\Phi_P}{dr}, \frac{1}{2\pi r} \frac{d\Phi_T}{dr}\right) + \left(0, \frac{\partial \tilde{\psi}}{\partial s}, -\frac{\partial \tilde{\psi}}{\partial \vartheta_R}\right); \tag{4.11}$$

the total field is given by the sum of an average field, represented by the first term, plus a fluctuating field with zero net flux.

5. Constrained minimization of magnetic energy

(*a*) *Standard flux tube*

Let us specify the relation between toroidal and poloidal flux. Let $V_r = \pi r^2 L$ be the partial volume of the tubular neighbourhood of radius r; the ratio of the partial to total volume is given by $V_r / V(\mathcal{T}) = (r/a)^2$. Now, let $f(r/a)$ be a monotonically increasing function of r/a; for example,

$$f(r/a) = \left(\frac{r}{a}\right)^\gamma, \quad (\gamma > 0); \tag{5.1}$$

where $\gamma = 2$ gives the standard ratio of partial to total volume. Denoting by $\Phi := \Phi_{\mathrm{T}}(a)$ the total flux, we have

$$\Phi_{\mathrm{T}}(r) = \left(\frac{r}{a}\right)^{\gamma} \Phi, \quad \Phi_{\mathrm{P}}(r) = h \left(\frac{r}{a}\right)^{\gamma} \Phi, \tag{5.2}$$

where h denotes the *magnetic field framing*, given by $(2\pi)^{-1}$ times the turns of twist required to generate the poloidal field from the toroidal field, starting from $\Phi_{\mathrm{P}} = 0$. A direct calculation of helicity in terms of fluxes shows that h is indeed the linking number Lk of the embedded field (see appendix A). A *standard* flux tube (cf. CM95) is defined by taking $\gamma = 2$.

(*b*) *Topological bounds on energy minima*

Relaxation of magnetic knots under topological constraints has been studied by several authors, including Arnold (1974), Freedman (1988), Moffatt (1990) and Freedman & He (1991). Various bounds on magnetic energy $M(t)$ and relationships between energy minima $M_{\min}$ and topological complexity of knot type were found by these authors. In particular, for zero-framed knots, Ricca (2008) has proven that:

Theorem 5.1. *Let K be a zero-framed, essential magnetic knot, embedded in an ideal fluid. Then, we have*

$$\text{(i)} \quad M(t) \geq \left(\frac{2}{\pi}\right)^{1/3} \frac{|H|}{V^{1/3}} = 0 \quad \textit{and} \quad \text{(ii)} \quad M_{\min} = \left(\frac{2}{\pi}\right)^{1/3} \frac{\Phi^2}{V^{1/3}} c_{\min}, \tag{5.3}$$

where $c_{\min}$ is the topological crossing number of K.

Note: results of theorem 5.1 refer to the definition of magnetic energy given by equation (2.4), which involves the coefficient $\frac{1}{2}$.

By theorem 2.1 $Lk = 0$ yields $H = 0$, hence for zero-framed knots the lower bound given by inequality (5.3)(i) simply reduces to state the positiveness of $M(t)$. Equation (5.3)(ii), however, puts in relation knot topology and magnetic energy minima through crossing number information. By comparing equation (5.3)(ii) with equation (1.1) we see that $c_{\min} = m(0)$. Relationship (5.3)(ii), though, is not exhaustive, because with the exception of the 3- and the 4-crossing knot, all other isotopes have several topologically distinct representatives (see §8). Hence, equality (5.3)(ii) cannot help to detect knot types of same $c_{\min}$ on the basis of their minimum energy level alone (see the example of figure 4). For these cases specific other detectors are necessary.

(*c*) *Constrained relaxation to groundstate energy*

We now look for the groundstate energy of magnetic knots by the minimization of the magnetic energy (2.4) under specific constraints, following the same approach of CM95. The minimum energy thus obtained provides an upper bound to the true minimum attainable in the absence of constraints. Let M^* and L^* denote the constrained minimum magnetic energy and the corresponding minimal knot length. We have,

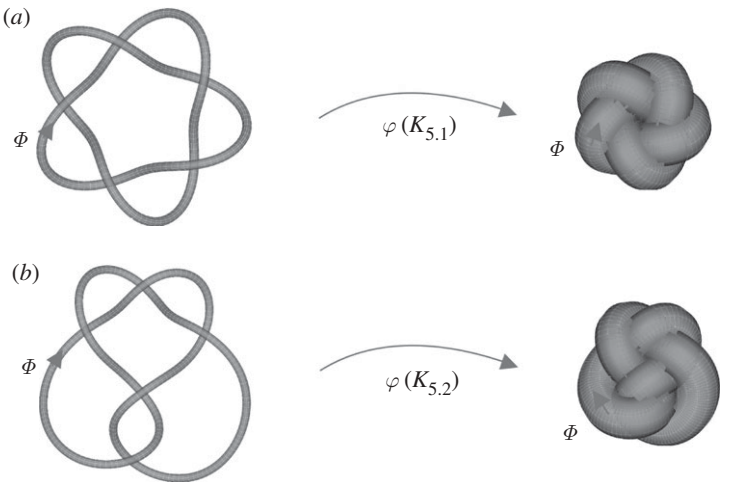

Figure 4. On the basis of equation (5.3)(ii) two different zero-framed knot types (for example the $K_{5.1}$ (a) and the $K_{5.2}$ (b) shown) with same volume, flux and $c_{\min}$, may both relax to the same minimum energy.

Theorem 5.2. *Let K be an essential magnetic knot in an ideal fluid, with signature $\{V, \Phi\}$ and magnetic field given by equation (4.11). We assume that*

(i) *$\{V, \Phi\}$ is invariant,*
(ii) *the circular cross section $\mathcal{S}$ is independent of the arc-length s,*
(iii) *$\widetilde{\psi}$ is independent of the arc-length s, and*
(iv) *the knot length L (or L^*) is independent of the knot framing h.*

Minimization of magnetic energy, constrained by (i)–(iv)*, yields*

$$M^* = \left(\frac{\gamma^2 L^{*2}}{8(\gamma - 1) V} + \frac{\gamma \pi h^2}{2L^*} \right) \Phi^2. \tag{5.4}$$

Proof. Let us express the magnetic energy (2.4) in the orthogonal coordinates $(r, \vartheta_{\mathrm{R}}, s)$,

$$M(t) = \frac{1}{2} \int_0^{L/k} \int_0^{2\pi} \int_0^a (B_{\vartheta_{\mathrm{R}}}^2 + B_s^2)\, \mathrm{d}r\, r \mathrm{d}\vartheta_{\mathrm{R}} k\, \mathrm{d}s. \tag{5.5}$$

As $\widetilde{\psi}$ is periodic in ϑ_{R}, we define $\Lambda(r, \vartheta_{\mathrm{R}}) = -\partial \widetilde{\psi} / \partial \vartheta_{\mathrm{R}}$ so as to have

$$\int_0^{2\pi} \Lambda(r, \vartheta_{\mathrm{R}})\, \mathrm{d}\vartheta_{\mathrm{R}} = 0. \tag{5.6}$$

By assumption (iii) and equation (5.6), we have

$$\begin{aligned} M(t) &= \frac{1}{2} \int_0^{L/k} \int_0^{2\pi} \int_0^a \left[\left(\frac{1}{L} \frac{\mathrm{d}\Phi_{\mathrm{P}}}{\mathrm{d}r} \right)^2 + \left(\frac{1}{2\pi r} \frac{\mathrm{d}\Phi_{\mathrm{T}}}{\mathrm{d}r} + \Lambda \right)^2 \right] \mathrm{d}r\, r\, \mathrm{d}\vartheta_{\mathrm{R}}\, k\, \mathrm{d}s \\ &= \frac{1}{2} \int_0^{L/k} \int_0^{2\pi} \int_0^a (\Lambda^2 + 2P\Lambda + Q)\, \mathrm{d}r\, r\, \mathrm{d}\vartheta_{\mathrm{R}}\, k\, \mathrm{d}s, \end{aligned} \tag{5.7}$$

where

$$P = \frac{1}{2\pi r}\frac{\mathrm{d}\Phi_{\mathrm{T}}}{\mathrm{d}r}, \quad Q = \frac{1}{L^2}\left(\frac{\mathrm{d}\Phi_{\mathrm{P}}}{\mathrm{d}r}\right)^2 + \frac{1}{4\pi^2 r^2}\left(\frac{\mathrm{d}\Phi_{\mathrm{T}}}{\mathrm{d}r}\right)^2. \tag{5.8}$$

Now we partially minimize M with respect to Λ, subject to the above constraints; let us introduce a Lagrange multiplier $\lambda(r)$ and minimize

$$\frac{1}{2}(\Lambda^2 + 2P\Lambda + Q) - \lambda(r)\Lambda(r, \vartheta_{\mathrm{R}}) \tag{5.9}$$

with respect to Λ; we obtain

$$\Lambda = \lambda(r) - P, \quad \int_0^{2\pi} (\lambda(r) - P)\,\mathrm{d}\vartheta_{\mathrm{R}} = 0. \tag{5.10}$$

From the second equation (5.10), we have

$$\lambda(r) = \frac{1}{2\pi}\int_0^{2\pi} P\,\mathrm{d}\vartheta_{\mathrm{R}}. \tag{5.11}$$

Now, by substituting the first equation (5.10) into (5.7), we get

$$M^* = \frac{1}{2}\int_0^{L^*/k}\int_0^{2\pi}\int_0^{a} \left(\lambda^2(r) - P^2 + Q\right)\,\mathrm{d}r\,r\,\mathrm{d}\vartheta_{\mathrm{R}}\,k\,\mathrm{d}s, \tag{5.12}$$

where $(\cdot)^*$ represents constrained minimization; from equations (5.8) and (5.11), we have

$$M^* = \frac{1}{2}\int_0^{a}\left[\frac{L^*}{2\pi r}\left(\frac{\mathrm{d}\Phi_{\mathrm{T}}}{\mathrm{d}r}\right)^2 + \frac{2\pi r}{L^*}\left(\frac{\mathrm{d}\Phi_{\mathrm{P}}}{\mathrm{d}r}\right)^2\right]\mathrm{d}r. \tag{5.13}$$

By taking $\Phi_{\mathrm{P}} = h\Phi_{\mathrm{T}}$ (cf. equation 5.2), the integral equation (5.13) reduces to

$$M^* = \int_0^{a}\left(\frac{\mathrm{d}\Phi_{\mathrm{T}}(r)}{\mathrm{d}r}\right)^2 \frac{L^{*2} + 4\pi^2 r^2 h^2}{4\pi r L^*}\,\mathrm{d}r. \tag{5.14}$$

Finally, by the first of equations (5.2) and straightforward integration, we have

$$M^* = \left(\frac{\gamma^2 L^*}{8\pi(\gamma - 1)a^2} + \frac{\pi\gamma h^2}{2L^*}\right)\Phi^2 = \left(\frac{\gamma^2 L^{*2}}{8(\gamma - 1)V} + \frac{\gamma\pi h^2}{2L^*}\right)\Phi^2, \tag{5.15}$$

where, in the last term, we have substituted $a = (V/\pi L^*)^{1/2}$ to express M^* in terms of the signature $\{V, \Phi\}$. ■

As we see, the constrained minimum energy depends on the length axis L^* and the square of the twist parameter h. For $\gamma = 2$, equation (5.15) reduces further to

$$M^* = \left(\frac{L^{*2}}{2V} + \frac{\pi h^2}{L^*}\right)\Phi^2. \tag{5.16}$$

At minimum energy, L^* is the minimal tube length of the relaxed 'tight' knot.

6. Constrained minimum energy by the SONO algorithm

As we see from equation (5.16), the constrained minimum energy of tubular knots is dictated by the tube minimal length. A useful measure of knot complexity is the knot *ropelength* L/R, where from now on (dropping the suffix $(\cdot)^*$) L and R will denote the minimal knot length and the radius of the maximal, circular cross section of the tightest knot configuration. For simplicity let us set $V=1$ and $\Phi=1$. Under a signature-preserving flow, from $V=1=\pi R^2 L$, and by elementary algebra, we have

$$1=\pi R^3\left(\frac{L}{R}\right) \quad \Longrightarrow \quad R=\left(\frac{1}{\pi(L/R)}\right)^{1/3}, \tag{6.1}$$

so that we can express the tight knot length L in terms of the ropelength L/R,

$$L=(L/R)\left(\frac{1}{\pi(L/R)}\right)^{1/3}=\left(\frac{(L/R)^2}{\pi}\right)^{1/3}. \tag{6.2}$$

Equation (5.16) can thus be re-written purely in terms of ropelength and internal twist, that is

$$M^*=\frac{(L/R)^{4/3}}{2\pi^{2/3}}+\frac{\pi^{4/3}h^2}{(L/R)^{2/3}}. \tag{6.3}$$

We can now calculate M^* by using algorithms that minimize ropelength for any given internal twist value. For this we can rely on one of the best algorithms available, namely the SONO algorithm, originally developed by Pieranski (1998) and collaborators.

(a) *The SONO algorithm*

The SONO algorithm is a numerical software implemented by Przybyl (2001) under the direction of Pieranski (1998), and subsequently improved by other collaborators. Technical details of this algorithm are widely available in the literature; the interested reader can consult several papers such as Pieranski *et al.* (2001), Pieranski & Przybyl (2002) and Baranska *et al.* (2004, 2005). We present here the ideas behind the algorithm and we highlight some critical aspects.

(i) *The perfect rope model*

The tightening process is based on the idea that the tubular knot is modelled by a perfectly flexible and infinitely hard, cylindrical rope. This means that the rope can be bent with zero force (no elastic energy stored) and it cannot be squeezed; hence, the rope cross section remains always perfectly circular. It is also assumed that the rope surface is perfectly frictionless and that the knot axis, together with its tangent, is everywhere smooth and continuous. This guarantees that the perpendicular cross section, given by a disc centred on the rope axis, is everywhere always well defined. Moreover, there is a control that enforces that perpendicular cross sections do not overlap to avoid self-intersections.

(ii) *Discretization*

The knot axis is standardly discretized piecewise linearly by a finite sequence of segments (beads) and vertices, to form a self-avoiding, polygonal knot K_P in $\mathbb{R}^3$. The tightening process starts from a non-equilateral polygon and proceeds to an equilateral configuration. The main difficulty here is to produce a polygonal knot that best reproduces the knot axis of the perfect rope. In finding the tightest (or *ideal*) configuration the initial ropelength provides an upper bound for the minimal value of the ideal configuration. To simulate the hard shell of the perfect rope, hard spheres are centred on the K_P vertices. Hence, the collection (union) of all these spheres generates a corrugated rope surface. This corrugation is made vanishingly small by increasing the number of vertices.

(iii) *Original procedure and subsequent improvements*

SONO's basic goal is to minimize the length of K_P, while ensuring that (a) the rope cells remain well-defined at all times, and (b) the rope cells do not overlap, while reducing K_P to the equilateral polygon (a rope cell is made by a sphere with two opposite cups appropriately removed). To avoid overlapping of contiguous cells a 'control curvature' (CC) procedure is implemented to control (bound) the angle between consecutive beads. This is complemented by a second procedure ('remove overlaps', RO) that controls the Euclidean distance between neighbouring (but not consecutive) vertices. In order to produce an equilateral polygon a third procedure ('equalize edges', EE) is implemented. Hence, the tightening process is achieved by an iterative application of the EE and RO procedures to minimize the differences in bead lengths and take account of emerging overlaps. The tightest configuration is thus given by an overlap-free, corrugated rope, centred on an equilateral polygonal knot. A preliminary version of SONO (Przybyl 2001) was followed by an improved version (Baranska *et al.* 2004), where a finer repositioning of the vertices is implemented through an appropriate displacement towards the local centre of curvature.

(*b*) *The problem of local/global minimum*

The tightening process forces the rope to change its configuration. The end state is achieved when further shortening of the ropelength is no longer possible, because this would create non-removable overlaps. When the number of beads is small, the rope surface is highly corrugated, and, upon tightening, this could allow different parts of the rope to be mutually entrenched in the grooves of the corrugation. This would then give false information on the end state, and, more specifically, on local minima of the ropelength (read 'energy'). As long as the number of cells is high, fine corrugation seems to prevent convergence to unrealistic local minima. However, at this stage a further readjustment of the vertices is not allowed and no procedure is implemented to explore possible neighbouring minima. Because global minimum configuration is not known *a priori* (and no analytical criterion is available), there is no certainty that the minimal ropelength configuration realized by the SONO tightening process corresponds actually to a global minimum.

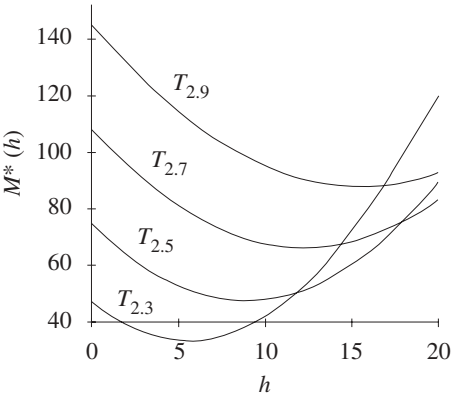

Figure 5. Groundstate energy spectrum of torus knots obtained by Chui & Moffatt (1995).

7. Constrained minimum energy of tight torus knots: comparative results

Orthogonal coordinates offer several advantages, one evidently being the economy and transparency of the calculations involved. Direct comparison of equation (5.16) with eqns (7.1), (7.12) and (7.13) of CM95 provides further evidence of this. Before comparing results, however, we should point out that eqns (5.19), (7.4), (7.9), (7.10) and (7.13) of CM95 contain typos and errors that need correction: the second integral on the r.h.s. of eqn (7.10), for instance, must be multiplied by L to be correct (also on dimensional grounds!). We can then proceed with the comparison: let $\epsilon = a/L$; from equation (5.16), we have

$$M^* = \frac{1}{\epsilon^2}\left(\frac{\gamma^2}{8\pi(\gamma-1)L} + \epsilon^2\frac{\pi\gamma h^2}{2L}\right)\Phi^2, \tag{7.1}$$

which, for $\gamma = 2$, reduces to

$$M^* = \frac{1}{\epsilon^2}\left(\frac{1}{2\pi L} + \epsilon^2\frac{\pi h^2}{L}\right)\Phi^2. \tag{7.2}$$

By comparing equation (7.2) with eqn (7.1) of CM95 (supplied by eqn (7.12) and the corrected (7.13)) we can see that the exact expression given by equation (7.2) corresponds to the contribution of eqn (7.12) and of one term only of the corrected (7.13), with higher order terms in the series expansion (7.1) left out. Here we should point out that the overall contribution of the cut-off terms, being these positive *and* negative, may well sum up to zero. In any case, the result of eqn (7.1) is then applied to study the groundstate energy of torus knot flux tubes (see §8 of CM95). Here the difficulty in analysing tight knot configurations was overcome by using standard torus knot equations (eqn (8.1) of CM95) and estimates on contact condition by some approximated form function (eqn (8.5) of CM95). The results obtained there are reproduced in figure 5.

In considering the relaxation to tight knot configuration, Chui & Moffatt (1995) made the implicit assumption that throughout the tightening process the knot axis would not have changed its initial geometry, the only change in time being

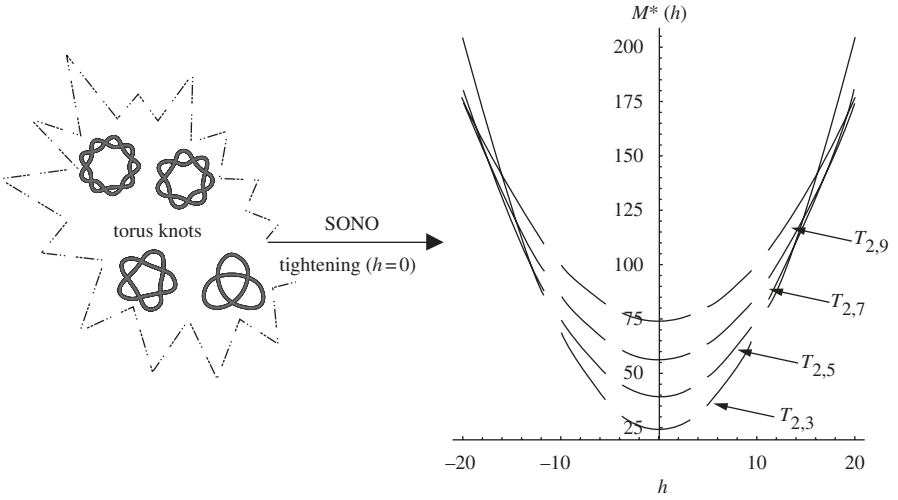

Figure 6. Constrained energy minima of torus knots given by equation (6.3). Data obtained by the knot tightening performed by the SONO algorithm correspond to $h=0$ (Przybyl 2001).

an average increase of the tubular knot circular cross section. However, we now know that this assumption is actually not legitimate. Numerical implementation of the global curvature concept to study tight knot configurations (Gonzalez & Maddocks 1999) and extensive numerical simulations made more recently by using the SONO algorithm (Pieranski & Przybyl 2002) shows that the knot axis changes shape during the tightening process, with progressive deformation owing to the change of curvature and torsion of $\mathcal{C}$ from the initial configuration to the final end-state (while keeping the cross section circular).

In the present case we can use the data on minimal ropelength of tight torus knots $T_{p,q}$ ($p>q$; p, q co-prime integers), obtained by the SONO algorithm simulation (see Przybyl 2001; pp. 47–49) for $h=0$. The results shown in figure 6 are given by equation (6.3) obtained by setting $V=1$, $\Phi=1$ (consistently with CM95). The curves are based on the SONO data at $h=0$ and then extrapolated according to equation (6.3). Note that, by doing so, we have assumed that minimal ropelength data remain independent from h. The quadratic dependence on the twist parameter h is thus evidenced by the family of parabolas. For direct comparison with results of CM95 (figure 5), we report only the constrained energy of torus knots of type $T_{2,q}(q=3,5,7,9)$; similar parabolic curves (at higher energy levels) are obtained for torus knots of higher topological complexity (see §8), such as the $T_{3,q}$ ($q>3$), $T_{4,q}$ ($q>4$), and so forth.

The two diagrams show some marked differences and some qualitative similarities. The first important difference is in the location of the minima that, in our case, are all centred at $h=0$. Consistently with equation (6.3), a non-zero framing (given by $h\neq 0$) yields an increase of the energy level, owing to the contribution of net twist to the groundstate energy. Moreover, take for example the energy curve of the trefoil knot $T_{2,3}$ in figure 5: considering that the average writhing number of the tight configuration is given by $Wr\approx 3.41$ (see, for example, the writhing number values calculated by SONO), the value

$h \approx 6$ (cf. CM95, p. 626) attained at the minimum is hard to justify, even by interpreting h in terms of internal twist (since by equations (2.6) and (A 12) in appendix A, $h = 0$ if and only if $|\mathrm{Tw}| = |\mathrm{Wr}|$). Moreover, the values at which the $T_{3,2}$ — topologically equivalent to the $T_{2,3}$ — attains its minimum energy (that with respect to $T_{2,3}$ are different in h and $M^{\star}$) seem to be completely wrong, considering that SONO tests on torus knots demonstrated (Pieranski 1998) that, for given p and q, $T_{q,p}$ and $T_{p,q}$ relax to the same tight configuration (hence, same ropelength and energy). Another difference is in the symmetry of the diagrams. The curves shown in figure 6 for $h \neq 0$ are extrapolated from SONO data at $h = 0$ according to equation (6.3). The assumption we made on the independence of ropelength from framing prevents us from stating that symmetry is actually preserved when this assumption is relaxed. Consistently with the diagrams of CM95, though, the diagrams in figure 6 show that, above a certain internal twist threshold $h_{\mathrm{cr}} = h_{\mathrm{cr}}(T_{p,q})$, minimum energy levels swap, reflecting the interplay between 'internal' and 'external' topological complexity—the former being associated with the field twist and the latter with the knot embedding in S^3. At zero framing ($h = 0$), however, internal twist vanishes and energy levels relate to knot topology in good agreement with equation (5.3)(ii).

8. Constrained groundstate energy of prime knots up to 10 crossings

We can estimate the constrained energy minima of prime knots up to 10 crossings by using data obtained by the SONO tightening process (Przybyl 2001, pp. 47–49). A word of caution is necessary here: as remarked by Przybyl and Pieranski,[1] one should bear in mind that the computed tight knot values tabulated are not rigorous and are subject to computational improvements. Assuming that the first decimal digit is correct, we inspect knot types of increasing complexity given by their c_{min}. For 3 and 4 crossings, there is only 1 knot type, but there are 2 for $c_{\mathrm{min}} = 5$, 3 for $c_{\mathrm{min}} = 6$, 7 for $c_{\mathrm{min}} = 7$, 21 for $c_{\mathrm{min}} = 8$, 49 for $c_{\mathrm{min}} = 9$ and 166 for $c_{\mathrm{min}} = 10$. As the distribution of the minimal length data produced by SONO is not, apparently, a monotonic function of c_{min}, the corresponding energy level results sometimes swapped between knot types of increasing c_{min}. To analyse data effectively we proceed in two steps. First, from each family of given c_{min}, we take the average minimal length ($\bar{L}$) out of the total number of knot representatives, and use this $\bar{L}$ to calculate the energy level of that family. The resulting curves, shown in figure 7, are therefore obtained by using equation (6.3) and extrapolating the diagrams from the SONO minimal average ropelength data obtained at $h = 0$.

To analyse the actual distribution of knots in relation to the groundstate energy we present a second diagram (see figure 8), where the median energy levels of figure 7 are reproduced on the r.h.s for reference. On the left-hand side we report the actual distribution of energy obtained for $h = 0$, centred on the relative average value (dashed lines). Each band shows the spread of energy for each knot family of given c_{min} (denoted by $K_{c_{\mathrm{min}}}$). For $h \neq 0$ these bands extend on either side of the vertical axis and are centred on their parabolic median (not shown in the figure).

[1]See http://fizyka.phys.put.poznan.pl/~pieransk/TablesUpTo9.html.

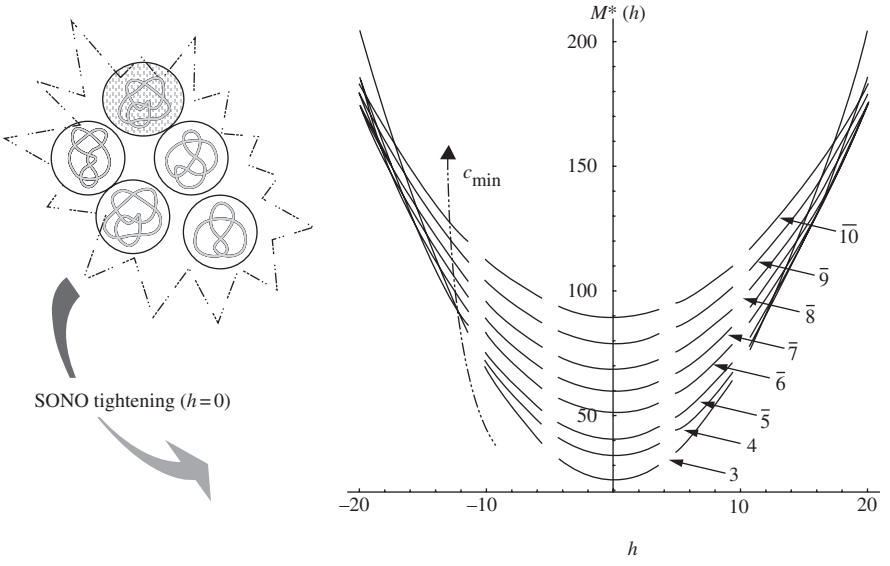

Figure 7. Constrained energy minima of prime knots of increasing complexity ($c_{\min}$) given by equation (6.3). Data obtained by the knot tightening performed by the SONO algorithm correspond to $h=0$ (Przybyl 2001). Overbar refers to data obtained by averaging values of tight knot lengths over the number of representatives within each family.

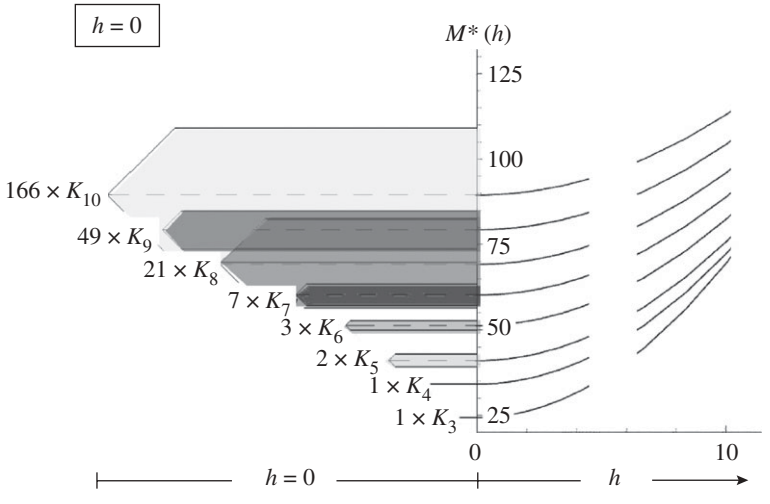

Figure 8. Constrained energy minima of knot representatives (on the right) are compared with the corresponding bands of energy (on the left) obtained for $h=0$. Results are based on the data currently available, obtained by the SONO tightening algorithm at $h=0$ (Przybyl 2001). Bands refer to the distribution of energy levels of knot representatives belonging to a given knot family, denoted by $K_{c_{\min}}$. There is only 1 knot type for the 3 and the 4 crossing families, whereas there are 3 for $c_{\min}=6$, 7 for $c_{\min}=7$, 21 for $c_{\min}=8$, 49 for $c_{\min}=9$ and 166 for $c_{\min}=10$.

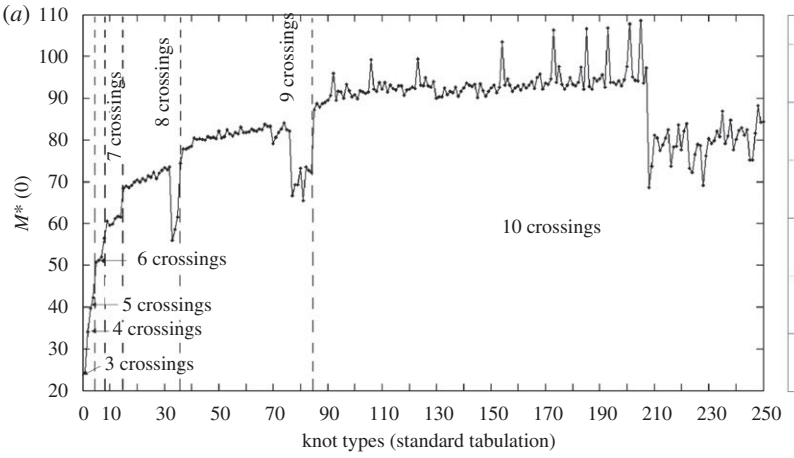

$c_{\min}$	outliers	M^* (0)
5	5.1	39.719
	5.2	42.297
6	6.1	50.734
	6.3	52.078
7	7.1	56.414
	7.6	61.713
8	8.18	55.948
	8.19	73.524
9	9.46	65.469
	9.39	84.079
10	10.124	68.566
	10.121	108.6

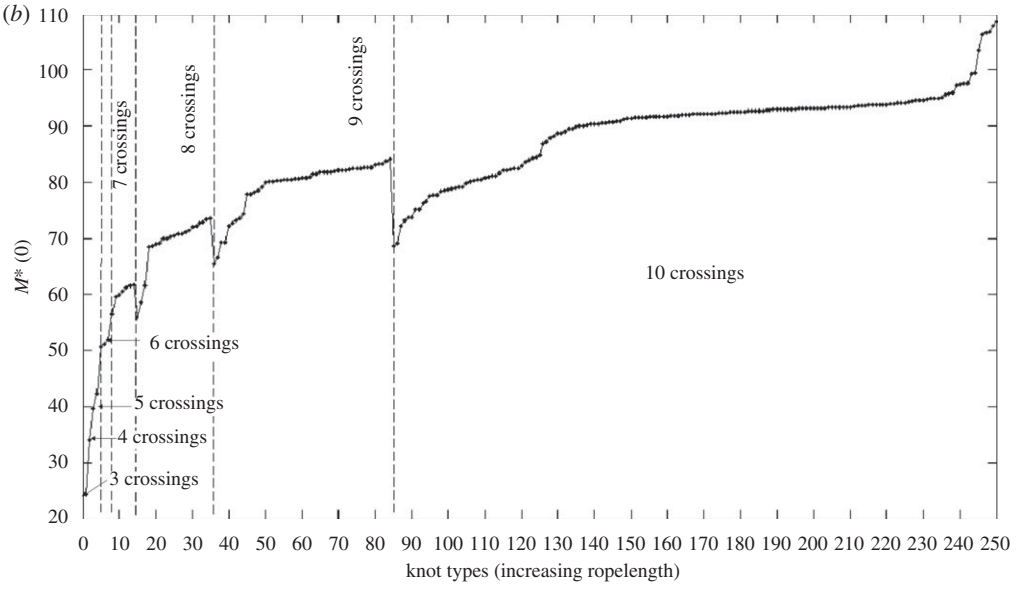

Figure 9. (*a*) Constrained groundstate energy of tight knots up to 10 crossings, based on data provided by the SONO algorithm; the knots are distributed according to standard knot tabulation with increasing crossing number. The table on the r.h.s. lists the knots (outliers) with minimum and maximum $M^*(0)$ (M^* at $h=0$) within each $c_{\min}$ family. (*b*) Constrained groundstate energy versus knot type; the knots are now distributed according to their minimal ropelength values.

According to current SONO data, one-to-one correspondence between constrained minimum energy and knot complexity holds up to knot $K_{8.18}$ (i.e. it extends to include the first 32 knot types): the minimal length of $K_{8.19}$ appears to be shorter than that of $K_{7.1}$. It is curious to notice that, according to standard (Rolfsen) knot tabulation, the knot representatives that break this correspondence are those (mostly non-alternating) listed in the last positions of the table: these are the last 3 in the 8-crossing family, the last 8 in the

9-crossing family, and, with the exception of 3 knots, the last 40 in the 10-crossing family. This is evidenced by figure 9*a*, which shows the energy distribution against knot types listed according to the standard knot tabulation. The table on the r.h.s. lists the knot outliers of each $c_{\min}$ family with minimum and maximum $M^*(h=0)$. By re-ordering the knot types of each $c_{\min}$ family in terms of increasing minimal ropelength we obtain figure 9*a*, which clearly demonstrates that, other than crossing number, ropelength is indeed a good detector of topological complexity.

9. Concluding remarks

The results presented in this paper on the groundstate energy of prime knots up to 10 crossings are based on a new, exact analytical expression for the constrained minima of magnetic energy. This is obtained as an improvement of previous work done by Chui & Moffatt (1995), by using appropriate orthogonal coordinates and standard variational methods. A magnetic knot is identified with a tubular knot filled by a magnetic field, decomposed in poloidal and toroidal components. The tubular knot is given by a tube centred on the knot axis with circular cross section, in which framing of the tubular knot is given by the linking of the field lines with the knot axis. By assuming volume and flux invariance, uniform circular cross section along the tube axis at all times, and independence of knot length from framing, we determine the constrained minimum magnetic energy functional (equation (5.4)), and show that for standard flux-tube the minimizer reduces further to a simple expression (equation (6.3)), function of ropelength and framing. Constrained minima are local minima for the magnetic relaxation process and provide an approximation from above to the actual minima. By using SONO data for tight knots we determine the groundstate energy spectrum of the first prime knots up to 10 crossings, and compare results for torus knots with previous work done by CM95. Comparison of diagrams shows some marked differences and some qualitative similarities: contrary to CM95, in the present case the constrained groundstate energy reaches its minimum at zero-framing ($h=0$), and the minimizer results an even function of h. This means that the minimizer for a given framing and its negative are simply mirror images.

Relaxation of basic constraints, numerical improvement of the tightening process and improved numerical accuracy can bring significant improvements on the energy bounds. The assumption of circular cross section certainly represents the strongest limitation to further minimization of energy and any relaxation of this constraint is likely to bring appreciable improvements on the minima. Evidently, this problem is paired with the difficulty of determining the 'free volume' of the interstices that survive to the minimization, and because these are evidently related to the number of crossings (Buck & Simon 1999), larger adjustments are expected for knots of greater topological complexity. Tight knot data may then be sensitive to specific implementation of the tightening process. Apart from the test case of the trefoil knot (Gonzalez & Maddocks 1999), there is no information on how different techniques, based on SONO, global curvature radius, or others, compare. Here too, significant improvements of energy minima may be achieved when particularly complex topologies are tested. Finally,

as work on trefoil knots demonstrates (Baranska *et al.* 2004), computational progress in numerical analysis (discretization techniques, error control, etc.) improves accuracy and this, in turn, is reflected on corrections to energy levels.

From a more general viewpoint a comparison between different techniques would be very beneficial. For instance, by using equation (5.3)(ii) and (6.3) (at $h=0$), Ricca (in press) has derived a new, lower bound for the ropelength of tight knots of any $c_{\min}$, improving the ropelength bound of Buck & Simon (1999), obtained by different methods. Existence of a global minimum in each isotopy class for minimizers that depend solely on ropelength has been established by Cantarella *et al.* (2002), and an extension of this result to include framing is, to the best of our knowledge, yet to be done. Alternative minimizers (for some 'twisto-elastic' energy) that depend on ropelength *and* framing are not available, so that a direct comparison with results obtained by different methods is not possible. The role of knot chirality, for example, that in the present context is simply demanded to ropelength minimization might be detected by minimizers of different type. This calls for more work by numerical simulations of knot tightening, for instance by implementing new procedures not only for the fine tuning of local minima but also for investigating the role of framing, and for inspecting symmetry issues in relaxed states.

In this sense, the present work should be considered as an important complement to current work on minimum ropelength of tight knots (Litherland *et al.* 1999; Cantarella *et al.* 2002) and properties of ideal knots (Gonzalez & De La Llave 2003). For applications, it has obvious implications for all those problems in magnetohydrodynamics that involve estimates on energy-complexity relations, especially in astrophysics, solar physics and plasma physics.

We would like to thank Rob Kusner and P. Pieranski for providing some useful information and for updating us on current work on the SONO algorithm.

Appendix A

Magnetic helicity, given by equation (2.5), can be written in terms of toroidal and poloidal flux. By using the orthogonal coordinates $(r, \vartheta_{\mathrm{R}}, s)$ we show that equation (2.5) reduces to equation (2.6) with $Lk=h$. In order to have $\Phi=0$ in $S^3\backslash\mathcal{T}$ and helicity gauge-invariant, we take $\mathbf{A}=(0, A_{\vartheta_{\mathrm{R}}}, A_s)$ such that

$$\int_0^{L/k} A_s(a,0,s)\, k\, \mathrm{d}s = 0. \tag{A 1}$$

Since $\mathbf{B}=(0, B_{\vartheta_{\mathrm{R}}}, B_s)$, we have

$$\mathbf{B} = \nabla \times \mathbf{A} = \frac{1}{rk} \det \begin{pmatrix} \hat{\mathbf{e}}_r & r\hat{\mathbf{e}}_{\vartheta_{\mathrm{R}}} & k\hat{\mathbf{t}} \\ \dfrac{\partial}{\partial r} & \dfrac{\partial}{\partial \vartheta_{\mathrm{R}}} & \dfrac{\partial}{\partial s} \\ 0 & rA_{\vartheta_{\mathrm{R}}} & kA_s \end{pmatrix}. \tag{A 2}$$

From equation (4.11), by equating corresponding components, we have

$$\left.\begin{aligned}\frac{1}{rk}\left[\frac{\partial(kA_s)}{\partial\vartheta_{\mathrm{R}}}-\frac{\partial(rA_{\vartheta_{\mathrm{R}}})}{\partial s}\right]&=0,\\ -\frac{1}{k}\frac{\partial(kA_s)}{\partial r}&=\frac{1}{L}\frac{\mathrm{d}\Phi_{\mathrm{P}}}{\mathrm{d}r}+\frac{\partial\widetilde{\psi}}{\partial s},\\ \frac{1}{r}\frac{\partial(rA_{\vartheta_{\mathrm{R}}})}{\partial r}&=\frac{1}{2\pi r}\frac{\mathrm{d}\Phi_{\mathrm{T}}}{\mathrm{d}r}-\frac{\partial\widetilde{\psi}}{\partial\vartheta_{\mathrm{R}}}.\end{aligned}\right\}\tag{A 3}$$

Straightforward integration of the last two equations gives

$$\left.\begin{aligned}A_s&=-\frac{1}{L}\Phi_{\mathrm{P}}(r)-\int_0^r\frac{\partial\widetilde{\psi}}{\partial s}\,\mathrm{d}\bar{r},\\ A_{\vartheta_{\mathrm{R}}}&=\frac{1}{2\pi r}\Phi_{\mathrm{T}}(r)-\int_0^r\frac{\partial\widetilde{\psi}}{\partial\vartheta_{\mathrm{R}}}\,\mathrm{d}\bar{r}.\end{aligned}\right\}\tag{A 4}$$

Now let

$$\eta(r,\vartheta_{\mathrm{R}},s)=\int_0^r\widetilde{\psi}(\bar{r},\vartheta_{\mathrm{R}},s)\,\mathrm{d}\bar{r},\tag{A 5}$$

single valued and periodic in s and ϑ_{R}; hence, equations (A 4) become

$$\left.\begin{aligned}A_s&=-\frac{1}{L}\Phi_{\mathrm{P}}(r)-\frac{\partial\eta}{\partial s}+C_1(\vartheta_{\mathrm{R}},s),\\ A_{\vartheta_{\mathrm{R}}}&=\frac{1}{2\pi r}\Phi_{\mathrm{T}}(r)-\frac{\partial\eta}{\partial\vartheta_{\mathrm{R}}}+C_3(\vartheta_{\mathrm{R}},s),\end{aligned}\right\}\tag{A 6}$$

where $C_1(\vartheta_{\mathrm{R}},s)$ and $C_3(\vartheta_{\mathrm{R}},s)$ are constants of integration: condition (A 1) is satisfied by setting $C_1(\vartheta_{\mathrm{R}},s)=\Phi_{\mathrm{P}}(a)/L$, and continuity of $\mathbf{A}$ at $r=0$ implies $C_3(\vartheta_{\mathrm{R}},s)=0$. Thus, we have

$$\left.\begin{aligned}A_s&=\frac{\widetilde{\Phi}_{\mathrm{P}}(r)}{L}-\frac{\partial\eta}{\partial s},\\ A_{\vartheta_{\mathrm{R}}}&=\frac{1}{2\pi r}\Phi_{\mathrm{T}}(r)-\frac{\partial\eta}{\partial\vartheta_{\mathrm{R}}},\end{aligned}\right\}\tag{A 7}$$

where $\widetilde{\Phi}_{\mathrm{P}}(r)=\Phi_{\mathrm{P}}(a)-\Phi_{\mathrm{P}}(r)$ is the complementary poloidal flux. Now let

$$H(r^*)=\int_{V^*(K)}\mathbf{A}\cdot\mathbf{B}\,\mathrm{d}^3\mathbf{x}=\int_0^{L/k}\int_0^{2\pi}\int_0^{r^*}(A_{\vartheta_{\mathrm{R}}}B_{\vartheta_{\mathrm{R}}}+A_sB_s)\,\mathrm{d}\bar{r}\bar{r}\,\mathrm{d}\vartheta_{\mathrm{R}}k\,\mathrm{d}s,\tag{A 8}$$

the helicity associated with the tubular neighbourhood of radius r^*. As in CM95, by using the equations above and direct integration, we have

$$H(r^*)=\int_0^{r^*}\left(\frac{\mathrm{d}\Phi_{\mathrm{T}}}{\mathrm{d}\bar{r}}\widetilde{\Phi}_{\mathrm{P}}-\frac{\mathrm{d}\widetilde{\Phi}_{\mathrm{P}}}{\mathrm{d}\bar{r}}\Phi_{\mathrm{T}}\right)\mathrm{d}\bar{r},\tag{A 9}$$

with total helicity given by

$$H=H(a)=\int_0^a\frac{\mathrm{d}\Phi_{\mathrm{T}}}{\mathrm{d}\bar{r}}(\Phi_{\mathrm{P}}(a)-\Phi_{\mathrm{P}}(\bar{r}))\,\mathrm{d}\bar{r}+\int_0^a\frac{\mathrm{d}\Phi_{\mathrm{P}}(\bar{r})}{\mathrm{d}\bar{r}}\Phi_{\mathrm{T}}\,\mathrm{d}\bar{r};\tag{A 10}$$

hence

$$H = 2\int_0^a \Phi_T \frac{d\Phi_P}{d\bar{r}}\, d\bar{r}. \tag{A 11}$$

By taking $d\Phi_P/dr = h(d\Phi_T/dr)$, magnetic helicity is given by

$$H = 2h\int_0^a \Phi_T \frac{d\Phi_T}{dr}\, dr = h\Phi^2. \tag{A 12}$$

Hence, equation (2.5) reduces to equation (2.6), with $h = Lk$.

References

Arnold, V. I. 1974 The asymptotic Hopf invariant and its applications. *Proc. Summer School in Differential Equations at Dilizhan*, pp. 229–256. Erevan, Armenia: Armenian Academy of Science (in Russian). [English translation: (1986) *Sel. Math. Sov.* **5**, 327–345.]

Baranska, J., Pieranski, P., Przybyl, S. & Rawdon, E. J. 2004 Length of the tightest trefoil knot. *Phys. Rev. E* **70**, 051810. (doi:10.1103/PhysRevE.70.051810)

Baranska, J., Pieranski, P. & Rawdon, E. J. 2005 Ropelength of tight polygonal knots. In *Physical and numerical models in knot theory*, vol. 36 (eds. J. A. Calvo *et al.*), pp. 293–321. Series on Knots and Everything. Singapore: World Scientific.

Bateman, G. 1978 *MHD instabilities*. Boston, MA: MIT Press.

Berger, M. A. & Field, G. B. 1984 The topological properties of magnetic helicity. *J. Fluid Mech.* **147**, 133–148. (doi:10.1017/S0022112084002019)

Buck, G. & Simon, J. 1999 Thickness and crossing number of knots. *Topol. Appl.* **91**, 245–257. (doi:10.1016/s0166-8641(97)00211-3)

Cantarella, J., Kusner, R. B. & Sullivan, J. 2002 On the minimum ropelength of knots and links. *Invent. Math.* **150**, 257–286. (doi:10.1007/S00222-002-0234-y)

Chui, A. Y. K. & Moffatt, H. K. 1995 The energy and helicity of knotted magnetic flux tubes. *Proc. R. Soc. Lond. A* **451**, 609–629. (doi:10.1098/rspa.1995.0146)

Freedman, M. H. 1988 A note on topology and magnetic energy in incompressible perfectly conducting fluids. *J. Fluid Mech.* **194**, 549–551. (doi:10.1017/S002211208800309X)

Freedman, M. H. & He, Z.-X. 1991 Divergence-free fields: energy and asymptotic crossing number. *Ann. Math.* **134**, 189–229. (doi:10.2307/2944336)

Gonzalez, O. & De La Llave, R. 2003 Existence of ideal knots. *J. Knot Theory Ramifications* **12**, 123–133. (doi:10.1142/s0218216503002354)

Gonzalez, O. & Maddocks, J. H. 1999 Global curvature, thickness, and the ideal shapes of knots. *Proc. Natl Acad. Sci. USA* **96**, 4769–4773. (doi:10.1073/pnas.96.9.4769)

Litherland, R. A., Simon, J., Durumeric, O. & Rawdon, E. 1999 Thickness of knots. *Topol. Appl.* **99**, 233–244. (doi:10.1016/S0166-8641(97)00210-1)

Mercier, C. 1963 Sur une representation des surfaces toroidales: applications aux equilibres magnetohydrodynamiques. *Nucl. Fusion* **3**, 89–98.

Moffatt, H. K. 1990 The energy spectrum of knots and links. *Nature* **347**, 367–369. (doi:10.1038/347367a0)

Moffatt, H. K. 2001 Some remarks on topological fluid mechanics. In *An introduction to the geometry and topology of fluid flows*, vol. 47 (ed. R. L. Ricca), pp. 3–10. NATO Science Series. II. Mathematics, Physics and Chemistry. Dordrecht, The Netherlands: Kluwer Academic Publisher.

Moffatt, H. K. & Ricca, R. L. 1992 Helicity and the Călugăreanu invariant. *Proc. R. Soc. Lond. A* **439**, 411–429. (doi:10.1098/rspa.1992.0159)

Pieranski, P. 1998 In search of ideal knots. In *Ideal knots*, vol. 19 (eds. A. Stasiak *et al.*), pp. 20–41. Series on Knots and Everything. Singapore: World Scientific.

Pieranski, P. & Przybyl, S. 2002 In search of the ideal trefoil knot. In *Physical knots: knotting, linking, and folding geometric objects in IR^3*, vol. 304 (eds. J. A. Calvo *et al.*), pp. 153–162. Contemporary Mathematics. Providence, RI: American Mathematical Society.

Pieranski, P., Przybyl, S. & Stasiak, A. 2001 Tight open knots. *Eur. Phys. J. E* **6**, 123–128. (doi:10.1007/s101890170012)

Przybyl, S. 2001 The search for the ideal knots and their properties. PhD thesis. (In Polish.) Poznan University of Technology, Poznan. http://fizyka.phys.put.poznan.pl/~pieransk/SylwesterPrzybyl-Thesis.pdf.

Ricca, R. L. 2008 Topology bounds energy of knots and links. *Proc. R. Soc. A* **464**, 293–300. (doi:10.1098/rspa.2007.0174)

Ricca, R. L. In press. New developments in topological fluid mechanics. *Nuovo Cimento C.*

Spivak, M. 1979 *A comprehensive introduction to differential geometry*, vol. 1. Houston, TX: Publish or Perish.

Stasiak, A., Katritch, V. & Kauffman, L. H. (eds) 1998 *Ideal knots*, vol. 19. Series on Knots and Everything. Singapore: World Scientific.

Woltjer, L. 1958 A theorem on force-free magnetic fields. *Proc. Natl Acad. Sci. USA* **44**, 489–491. (doi:10.1073/pnas.44.6.489)